

Seismic protection of smart base-isolated structures using negative stiffness device and regulated damping

Arash Bahar*, Mohsen Salavati-Khoshghalb^a and Seyed Mehdi Ejabati^b

Department of Civil Engineering, Faculty of Engineering, University of Guilan, Rasht, Iran

(Received July 4, 2017, Revised February 14, 2018, Accepted February 19, 2018)

Abstract. Strong seismic events commonly cause large drift and deformation, and functionality failures in the superstructures. One way to prevent functionality failures is to design structures which are ductile and flexible through yielding when subjected to strong ground excitations. By developing forces that assist motion as “negative stiffness forces”, yielding can be achieved. In this paper, we adopt the weakening and damping method to achieve a new approach to reduce all of the structural responses by further adjusting damping phase. A semi-active control system is adopted to perform the experiments. In this adaptation, negative stiffness forces through certain devices are used in weakening phase to reduce structural strength. Magneto-rheological (MR) dampers are then added to preserve stability of the structure. To adjust the voltage in MR dampers, an inverse model is employed in the control system to command MR dampers and generate the desired control forces, where a velocity control algorithm produces initial required control force. An extensive numerical study is conducted to evaluate proposed methodology by using the smart base-isolated benchmark building. Totally, nine control systems are examined to study proposed strategy. Based on the numerical results of seven earthquakes, the use of proposed strategy not only reduces base displacements, base accelerations and base shear but also leads to reduction of accelerations and inter story drifts of the superstructure. Numerical results shows that the usage of inverse model produces the desired regulated damping, thus improving the stability of the structure.

Keywords: weakening and damping; negative stiffness device; MR damper; inverse model; velocity control algorithm; smart base-isolated

1. Introduction

Base isolation systems are one of the widely implemented and the most successful techniques to mitigate the effects of earthquakes on buildings and their vulnerable contents in the past four decades (Charleston *et al.* 1987, Skinner *et al.* 1993, Naeim and Kelly 1999, Christopoulos *et al.* 2006, Sorace and Terenzi 2008). Base isolators decouple the superstructure from ground by installing certain devices of low stiffness in between. Bearings in various types have been used to reduce the forces transmitted from the seismic ground motion in base isolation systems (Naeim and Kelly 1999). Using these devices leads to an increase in the fundamental period of the structures.

Base isolation systems under near-fault, high-velocity, long-period ground motions, however, result in large base displacements (Hall *et al.* 1995, Jangid and Kelly 2001). Furthermore, these large base displacements can lead to buckling of the isolator devices or in some cases

pounding with adjacent structures. Thus, these systems require sufficient energy dissipation capacity through damping devices and, at the same time, adequate rigidity and stability to make the isolated building adoptable under general service loading or low seismic motions (Christopoulos *et al.* 2006, Sorace and Terenzi 2008).

In order to reduce base displacements, it is a common practice to incorporate supplemental energy dissipation devices. The structure with adjustable control devices implemented in the isolation system is called smart base isolated structure. Passive system consists of a base isolation system augmented by tune mass dampers, fluid viscous dampers, viscoelastic dampers, or friction dampers, as passive devices (Soong 1990). Although the installation of supplementary passive damping devices can reduce base displacement in the seismic events, it may increase inter-story drifts and floor accelerations (Makris 1997, Kelly 1999). In a fully active system that consists of a base isolation system augmented by sensors, controllers, and actuators (e.g., active mass dampers, active tendon and bracing systems), sensors are used to measure external excitations and structural responses; controllers are used to process the information measured by sensors and compute output control forces using a given control algorithm; actuators are used to generate the required forces (Soong 1990).

In this paper, we implement a semi-active control system, in which the base isolated system is augmented by Magneto-rheological (MR) dampers (Dyke *et al.* 1996,

*Corresponding author, Assistant Professor

E-mail: bahar@guilan.ac.ir

^a Master of Engineering

E-mail: mkhoshghalb@msc.guilan.ac.ir

^b Master of Engineering,

E-mail: ejabati@msc.guilan.ac.ir

Spencer *et al.* 1996, Dyke *et al.* 1998). Semi-active systems only require nominal energy sources like batteries to modify properties of MR dampers in real time, while active systems use massive external energy sources for actuators to produce opposite forces. Active systems also entail extra costs as capital and maintenance costs, and suffer from stability issues (Jung *et al.* 2006, Yang 2001, Bossis *et al.* 2003). Semi-active control systems present both the reliability of passive control systems in power failure cases, and adaptability characteristics of active control systems.

To solve displacement and acceleration issues as mentioned above, a new concept of Weakening and Damping (WeD) is introduced by Reinhorn *et al.* (2005) and Viti *et al.* (2006). In the WeD concept, the weakening phase reduces the strength and stiffness by disconnecting frames or walls in the superstructure. Then, the damping phase preserves the structural stability by introducing supplemental damping devices that protect superstructure from large deformations and displacements. The weakening phase can be achieved by implementing various devices that produce mechanical forces in the same direction of the imposed displacement. Generally, the weakening phase as an opposite strategy to strengthening the superstructure is applicable for buildings that have contained overstressed components and foundation supports, as well as weak brittle components.

Lemura and Pradono (2009) proposed pseudo-negative stiffness (PNS) dampers, which produce negative-stiffness hysteretic loops. They examined PNS dampers in both active and semi-active control systems, in which a linear input voltage is used to adjust PNS dampers. It should be noted that PNS dampers cannot produce negative stiffness forces in the same direction of the imposed displacement, and cannot reduce absolute acceleration for long-period structures.

Nagarajaiah *et al.* (2010) introduce true negative stiffness to produce forces that help motion in the desired direction. To generate true negative stiffness, they implement precompressed springs as adaptive negative stiffness devices (NSDs) for pushing the structure in the same direction of the imposed displacement. The NSDs are then implemented in an adaptive negative stiffness system by combining the NSDs with passive dampers. Sarlis *et al.* (2011) and Sarlis *et al.* (2012) present extensive studies of using the NSDs in the seismic protection of structures. In these studies, the reduction of apparent global lateral stiffness by implementing NSDs are validated. Thus, NSDs provide the desired true horizontal negative stiffness, while leaving the vertical stiffness intact. Moreover, the actual stiffness of structure remains unchanged. However, the NSDs provide variable stiffness that alternatively produce positive stiffness in large deformations.

Recently, the performance of NSDs have examined more extensively by Pasala *et al.* (2012) and Attary *et al.* (2012, 2013, 2015) and Attary *et al.* (2015a) in bridge structures. Attary *et al.* (2015a) proposed a new passive seismic response control device to produce negative stiffness forces using mechanical mechanism. The combination of negative stiffness and passive damping devices provides further control for seismic protection. In

Attary *et al.* (2015b) authors developed a rotation-based mechanical adaptive passive device which mechanically modifies stiffness either by adding positive or negative stiffness using different types of rotational elements.

In the present paper, an innovative strategy has presented for seismic protection of buildings by developing an adaptive semi-active control system. In this control system the concept of true negative stiffness is implemented in the smart base-isolation system. In contrast to (Sarlis *et al.* 2011, 2012) that use passive dampers, MR dampers are used in a semi-active control framework. To command MR dampers in varying seismic levels, an inverse model is implemented to adjust and further control necessary forces in the semi-active control system. Overall, by adjusting the damping responses of the protective system, a *Weakening and Regulated Damping* (WeRD) technology is obtained.

2. The weakening and regulated damping approach in the semi-active control systems

2.1 Weakening phase using negative stiffness device

In this section, we represent the main future of the Negative Stiffness Devices (NSDs) in order to weaken the structural elements. As opposed to a positive stiffness element, in the concept of true negative stiffness the NSD helps motion and displacement of the superstructure in the same direction imposed by seismic event (see e.g., Sarlis *et al.* (2011) for more details). We briefly express the working principle of NSD described in Sarlis *et al.* (2011, 2012). As presented in Sarlis *et al.* (2012), the effect of adding NSDs augmented by dampers can be shown in the force-displacement plots of Fig. 1. In Fig. 1(a), green line represents base isolation force; purple line represents damping force, and red line represents NSD force. Fig. 1(b) shows the assembly stiffness, in which NSDs are only employed whenever the displacement becomes greater than x_1 . Using NSDs (i.e., true negative stiffness), assembly stiffness is reduced to $k_a = k_e - k_n$. Although base shear is reduced in the structure with NSDs, the maximum deformation of whole system will be significantly increased. To reduce large displacement, damping device is set in parallel to the NSD, as shown in Fig. 1(c).

As implemented by Sarlis *et al.* (2011) and shown in Fig. 2 the NSD is composed of a vertical pre-compressed spring in the center of the device, and two horizontal gap spring assemblies on the bottom. The combination of frame and plates hold these elements integrated. The pre-compressed spring is in its minimum length when the NSD is un-deformed. When the device is at its deformed configuration, the pre-compressed spring produces a force in the direction of the displacement and acts to augment further motions.

In addition, the gap spring assemblies alternatively generate a bilinear elastic positive stiffness. Therefore, in small displacements (i.e., displacements less than x_1 in Figs. 1(b) and 1(c)), the gap spring assemblies counteracts with negative force/stiffness generated by NSD to stabilize

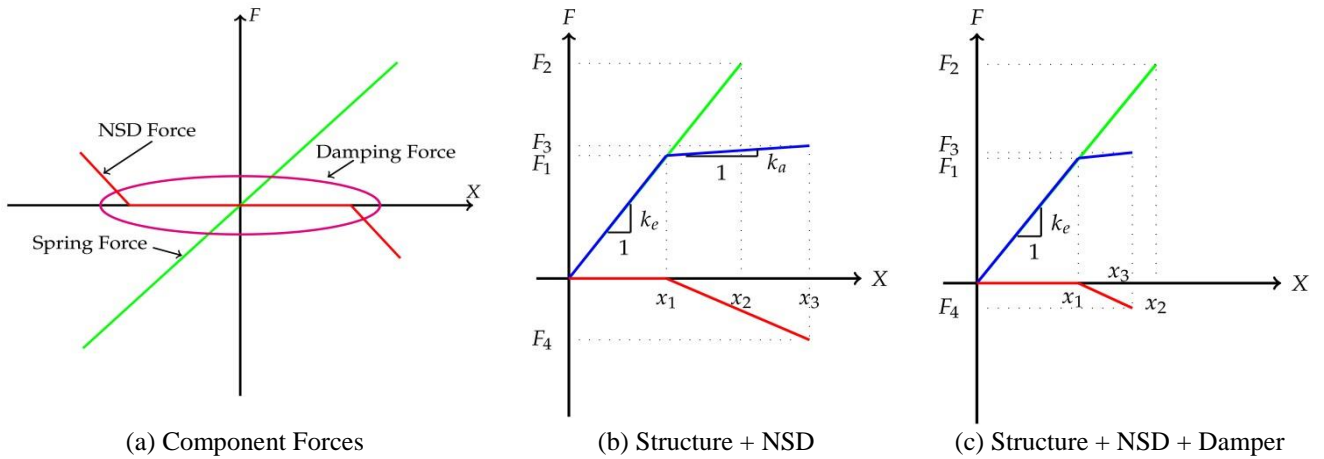


Fig. 1 Working Principle of NSD, see for more details Sarlis *et al.* (2011)

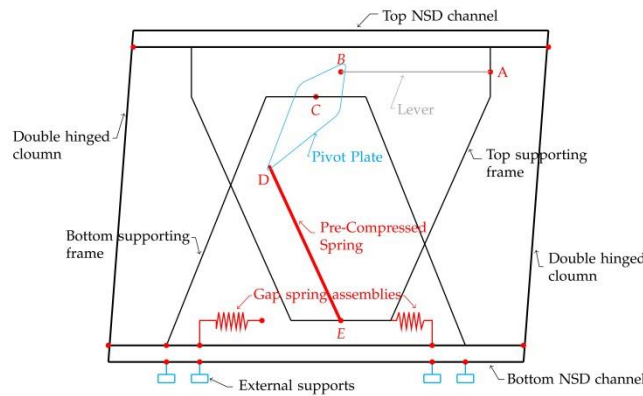


Fig. 2 Negative Stiffness Devices (Sarlis *et al.* 2011)

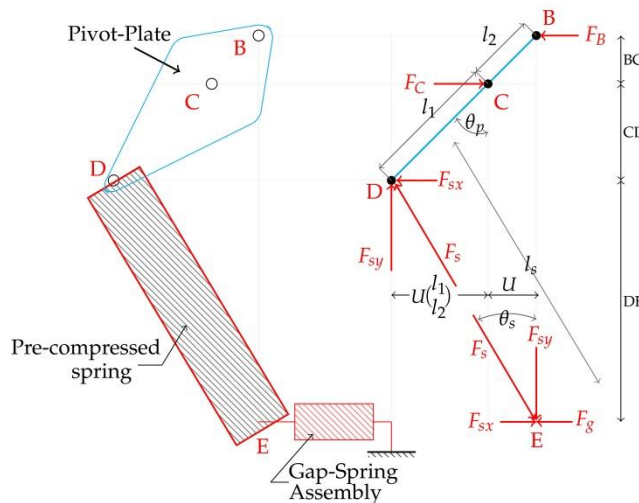


Fig. 3 Forces acting on pivot plate (Sarlis *et al.* 2011)

overall stiffness close to zero. For displacements more than x_1 , the gap spring assemblies softens drastically and then can engage the pre-compressed spring to generate true negative stiffness. More details can be seen in force-

displacement Figure where, for displacements $|x| > |x_1|$ NSD is engaged.

In Fig. 3, the schematic diagram of the device is shown after exerting a displacement on the top of it. The imposed

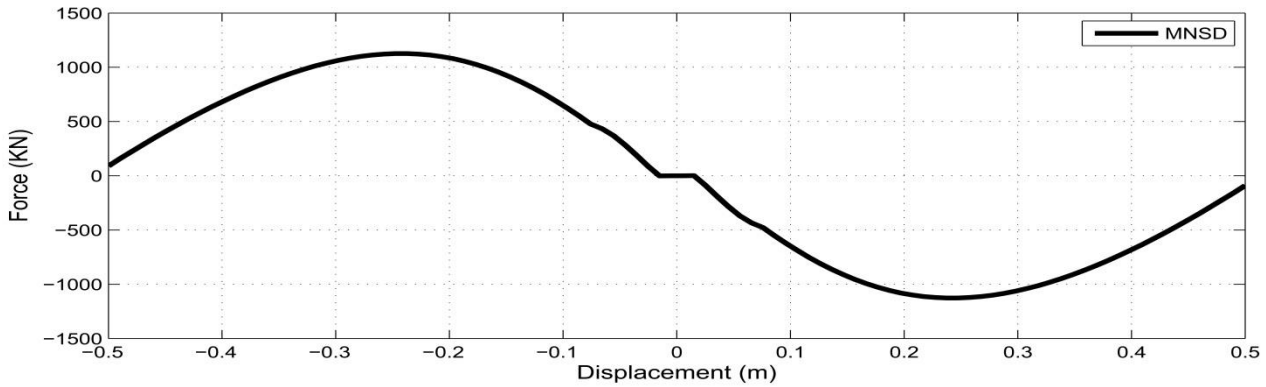


Fig. 4 Force versus displacement plot for MNSD

displacement by the lever on the top of the pivot plate (point B) lead to rotating the pivot plate about point C, and makes point D moves in the inverse direction rather than the imposed displacement. Movements in the points D and E deviate pre-compressed spring from vertical position, which in consequent, generates negative stiffness for further motion.

NSDs is used in an experimentally base-isolated structure with passive dampers. This paper is going to apply the NSDs devise in a benchmark base-isolated building with a well tunned semi-active control strategy. To do this, magnitude of the elements of NSDs and its functional range has calibrated for this new building, and refer it as Modified

Negative Stiffness Device (MNSD) in the rest of the paper.

A description of variables in MNSD are presented in Table 1. Also force-displacement plot for MNSD is shown in Fig. 4 (refer to Sarlis *et al.* (2012) for basic equations of NSDs).

2.2 Structural model of the base isolated system

The benchmark problem proposed by Narasimhan *et al.* (2006) is used to examine the efficiency of semi-active control system for the seismic response of the buildings.

Table 1 Variable description

Quantity	Value
Distance from spring pin to fixed pin	$l_1 = 0.11m$
Distance from lever pin to fixed pin	$l_2 = 0.055m$
Spring length	$l_p = 1.5m$
Spring rate	$K_s = 2057.06KN/m$
Preload	$P_{in} = 241.66KN$
Gap opening	$d_{gap} = 0.0165m$
Gap Spring Assembly Stiffness for $u < d_{gap}$	$K_{g,1} = 50.177KN/m$
Secondary Spring Assembly Stiffness $u > d_{gap}$	$K_{g,2} = 17.857KN/m$

The benchmark structure is a base-isolated eight-story, steel-braced framed building, 82.4-m long and 54.3-m wide, similar to existing buildings in Los Angeles, California. The floors 1-6 are in the form of L-shaped plan as shown in Fig. 5. The floors 7 and 8 are in the rectangular form. The superstructure is installed on a concrete base that is isolated by base isolators. The superstructure members, such as beam, column, bracing, and floor slab are modeled in detail. The floor slabs and the base are assumed to be rigid in plane. The superstructure and the base are modeled using three degrees of freedom (DOF) per floor at the center of mass. The combined model of the superstructure (24 DOF) and isolation system (3 DOF) consists of 27 degrees of freedom. Several isolation elements are included such as friction pendulum bearings and linear elastomeric bearings. Totally, 92 base isolators are integrated below the superstructure's base. The position of structural control devices shown in Fig. 6. The equations of motion for the elastic superstructure are expressed in the following form (Narasimhan *et al.* 2006)

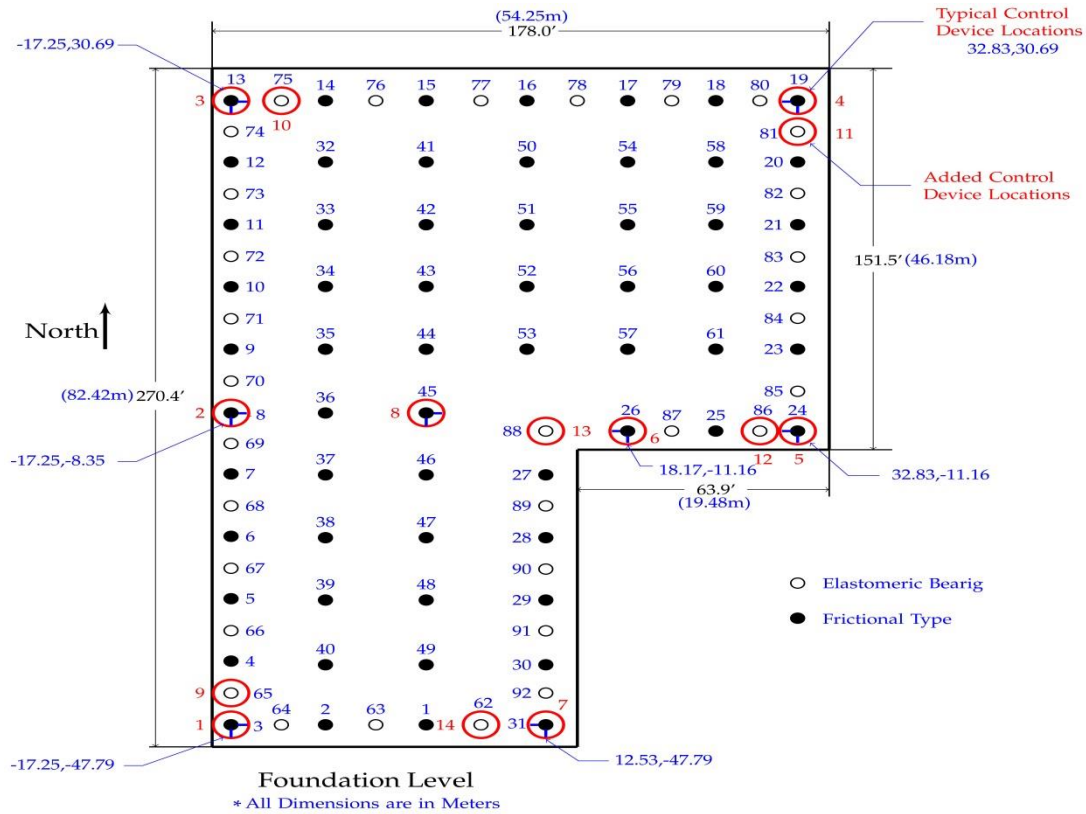
$$M_{n \times n} \ddot{U}_{n \times 1} + C_{n \times n} \dot{U}_{n \times 1} + K_{n \times n} U_{n \times 1} = -M_{n \times n} R_{n \times 3} (\ddot{U}_g + \ddot{U}_b)_{3 \times 1} \quad (1)$$

where, n is three times the number of floors (excluding base), M is the superstructure mass matrix, C is the superstructure damping matrix in the fixed base case, K is the superstructure stiffness matrix in the fixed base case and R is the matrix of earthquake influence coefficients, i.e., the matrix of displacements and rotation at the center of mass of the floors resulting from a unit translation in the X and Y directions and unit rotation at the center of mass of the base.

Furthermore, \ddot{U} , \dot{U} and U represent the floor acceleration, velocity and displacement vectors relative to the base, \ddot{U}_b is the vector of base acceleration relative to the ground and \ddot{U}_g is the vector of ground acceleration.

The equations of motion for the base are as follows (Narasimhan *et al.* 2006)

$$R_{3 \times n}^T M_{n \times n} \left[\left(\ddot{U} \right)_{n \times 1} + R_{n \times 3} \left(\ddot{U}_g + \ddot{U}_b \right)_{3 \times 1} \right]_{n \times 1} + M_{b3 \times 3} \left(\ddot{U}_g + \ddot{U}_b \right)_{3 \times 1} + C_{b3 \times 3} \dot{U}_{b3 \times 1} + K_{b3 \times 3} U_{b3 \times 1} + f_{b3 \times 1} + f_{c3 \times 1} = 0 \quad (2)$$


 Fig. 5 Benchmark problem building (Narasimhan *et al.* 2006)

where, M_b is the diagonal mass matrix of the rigid base, C_b is the resultant damping matrix of viscous isolation elements, K_b is the resultant stiffness matrix of elastic isolation elements, f_b is the vector containing the nonlinear bearing forces and f_c is the vector containing the control forces.

Re-writing the motion equations in the state-space form results in (Narasimhan *et al.* 2006)

$$\begin{aligned} \dot{X}(t) &= AX(t) + Bu(t) + B^* F_B(t) + E\ddot{U}_g(t) = \\ &g(X, u, \ddot{U}_g), \quad X = \{U^T U_b^T \dot{U}^T \dot{U}_b^T\}^T \\ A &= \begin{bmatrix} 0 & 1 \\ -\overline{M}^{-1}\overline{K} & -\overline{M}^{-1}\overline{C} \end{bmatrix}, \quad u = \begin{bmatrix} 0 \\ f_c \end{bmatrix} \\ E &= \begin{bmatrix} 0 \\ -\overline{M}^{-1} \begin{Bmatrix} MR \\ R^T MR + M_b \end{Bmatrix} \end{bmatrix}, \quad \overline{K} = \begin{bmatrix} K & 0 \\ 0 & K_b \end{bmatrix} \\ B &= B^* = \begin{bmatrix} 0 \\ -\overline{M}^{-1} \begin{Bmatrix} 0 \\ 1 \end{Bmatrix} \end{bmatrix}, \quad F_B = \begin{bmatrix} 0 \\ f_B \end{bmatrix} \\ \overline{M} &= \begin{bmatrix} M & MR \\ R^T M & R^T MR + M_b \end{bmatrix}, \quad \overline{C} = \begin{bmatrix} C & 0 \\ 0 & C_b \end{bmatrix} \end{aligned} \quad (3)$$

Where, C is the damping matrix of superstructure, C_b is the damping matrix of linear isolators, K is the

stiffness matrix of superstructure, K_b is the stiffness matrix of linear isolators, R is the matrix of earthquake coefficient, \ddot{U}, \dot{U}, U are respectively the floor acceleration, floor velocity, and floor displacement vectors, \dot{U}_b is the base acceleration vector, \ddot{U}_g is the ground acceleration vector, M is the superstructure mass matrix, M_b is the base mass matrix, f_B is the forces vector of nonlinear isolators, and f_c is the forces vector of control devices as dampers and NSDs. The state-space Eq. (3) will be solved using explicit Runge-kutta method for the numerical integration of the initial value problem.

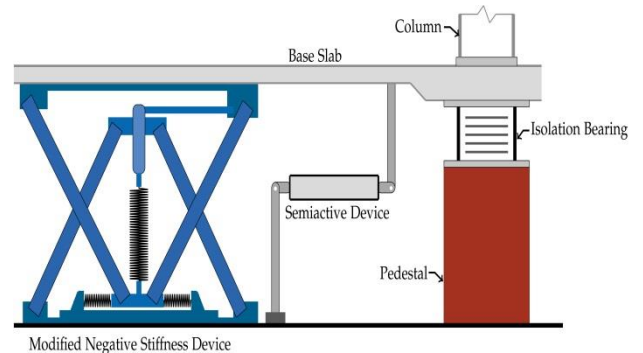


Fig. 6 Position of structural control devices

2.3 Regulated damping phase using an inverse model

In this paper, MR dampers are employed as the smart semi-active control devices which can generate necessary damping forces (Bahar *et al.* 2010). More precisely, the control forces will be applied at the base through manipulation of the command voltage of the MR dampers. The extended Bouc-Wen model used to command MR damper is as follows (Bahar *et al.* 2010)

$$\Phi_e(X, \dot{X}, W)(t) = K_x(v)X(t) + K_{\dot{x}}(v)\dot{X}(t) + K_W(v)W(t) \tag{4}$$

$$\dot{W}(t) = \rho(\dot{X}(t) - \sigma|\dot{X}(t)||W(t)|^{n-1}W(t) + (\sigma - 1)\dot{X}(t)|W(t)|^n) \tag{5}$$

Where $\Phi_e(X, \dot{X}, W)(t)$ is the output force of MR damper, $\dot{X}(t)$ and v are the velocity and voltage, respectively. The state variable $W(t)$ has not a physical meaning so that it is not accessible to be measured. The system parameters which are voltage-dependent, are $K_x(v) > 0$, $K_{\dot{x}}(v) > 0$, $K_W(v) > 0$, $\rho > 0$, $\sigma > 1/2$ and $n \geq 1$. It should be noted that the term $K_x(v)X(t)$ which represents a linear elastic force is added in the extended format of Bouc-Wen model. The second and third terms in Eq. (4) express the viscous and dry frictions of MR damper.

The velocity control algorithm is used because it provides better performance as shown in Bahar *et al.* (2010). The required command voltage can be computed as (Bahar *et al.* 2010)

$$v(X, \dot{X}, \Phi_e) = \frac{\Phi_e - K_x X(t) - K_{\dot{x},a} \dot{X}(t) - K_{W,a} \text{sgn}(\dot{X}(t))}{K_{\dot{x},b} \dot{X}(t) + K_{W,b} \text{sgn}(\dot{X}(t))} \tag{6}$$

Table 2 Parameters of inverse model (Bahar *et al.* 2010)

Parameter	Value	
K_x	207	
$K_{\dot{x}}$	$K_{\dot{x},a}$	89.64
	$K_{\dot{x},b}$	292
$K_{W,a}$	$0 \leq v < 0.52$	65.2
	$0.52 \leq v < 0.9$	902.1
	$0.9 \leq v < 1$	349.1
$K_{W,b}$	$0 \leq v < 0.52$	1720.8
	$0.52 \leq v < 0.9$	109.1
	$0.9 \leq v < 1$	715.3

$$v(X, \dot{X}, \Phi_e) = \frac{\Phi_e - K_x X(t) - K_{\dot{x},a} \dot{X}(t) - K_{W,a} \text{sgn}(\dot{X}(t))}{K_{\dot{x},b} \dot{X}(t) + K_{W,b} \text{sgn}(\dot{X}(t))} \tag{6}$$

where, $v(X, \dot{X}, \Phi_e)$ is voltage, $K_{\dot{x}}(v) = K_{\dot{x},a} + K_{\dot{x},b}$ is linear, $K_W(v)$ is a piecewise nonlinear function, and $K_{\dot{x},a}$, $K_{\dot{x},b}$, $K_{W,a}$, $K_{W,b}$ are defined in Table 2. Also, an initial force F for inverse model is set by following relation

$$F = 650\dot{X}(t) \tag{7}$$

This leads to produce more voltage for MR dampers and then more damping forces.

3. Semi-active control design in SIMULINK environment

To simulate the benchmark problem augmented by the MNSD and the inverse model, the control block diagram is simply implemented by modifying the SIMULINK block in the work by Narasimhan *et al.* (2006) as shown in Fig. 7. The modifications to the SIMULINK block are added in gray blocks and are detailed in Figs. 8 and 9. The base displacement in the two directions provide an input pair for MNSD block, available from measurement. Then, the MNSD force in each direction is computed separately. Finally, the two MNSD directional forces are integrated in a single force vector as the resulting output of the MNSD block. For each MR damper and each direction, an inverse model adjusts the control forces as shown in Fig. 9.

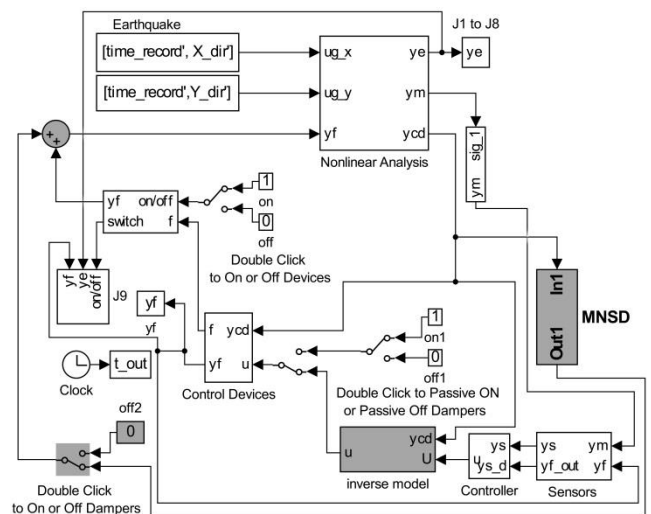


Fig. 7 SIMULINK block diagram for simulations with inverse model and MNSD

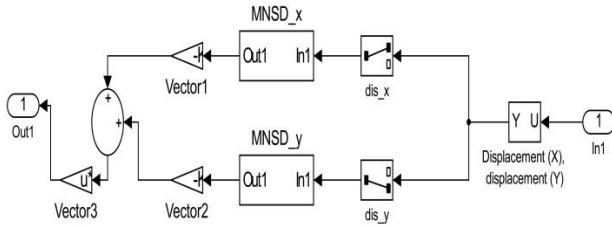


Fig. 8 MNSD block implemented in Fig. 7

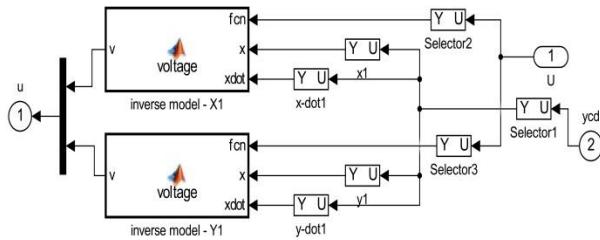


Fig. 9 Inverse model block implemented in Fig. 7 for MR dampers in each location

Three inputs are considered for each inverse model including (i) the control forces computed by the controller for MR damper; (ii) base displacement; and (iii) base velocity in the two directions. After computing the necessary voltage using Eq. (6) to generate necessary forces, the output of inverse model is presented by u . In addition, two on-off switches for MNSD and passive control blocks are added.

4. Numerical results

To investigate the effectiveness of the approach proposed in this paper, the smart base-isolated benchmark building Narasimhan *et al.* (2006) is employed. Nine different systems consisting of different combination of devices are examined to protect the superstructure as follows:

- System 1: Combination of Elastomeric Linear Bearings (LBs) and MR dampers, managed with inverse model
- System 2: Set of LBs with MR dampers as in Narasimhan *et al.* (2006)
- System 3: LBs with MNSDs
- System 4: LBs and MR dampers, managed with inverse model combined with MNSDs
- System 5: LBs and MR dampers, in passive-off case combined with MNSDs
- System 6: LBs and MR dampers, in passive-on case combined with MNSDs
- System 7: LBs with active control
- System 8: LBs with active control and MNSDs.
- System 9: LBs and MR dampers, in passive-on case Nagarajaiah and Narasimhan (2006)

Then, the efficiency of each control system is measured using five criteria $J1$, $J3$, $J4$, $J5$ and $J8$ as presented by

Pasala *et al.* (2012).

The results of nine control systems are summarized in Tables 3 and 4, for the fault normal (FN) and the fault parallel (FP) components of earthquakes exerting in two directions. Then, Tables 3 and 4 are compared with two limit cases as passive off (i.e., system 5) and passive on (i.e., system 6), which correspond to the zero voltage and maximum constant voltage cases. In system 9 we considered a passive on case without MNSDs. The results are also compared with system 3, system 1, and system 2 as in Narasimhan *et al.* (2006).

The smart base-isolated benchmark structure is simulated for seven earthquakes (i.e., Newhall, Sylmar, El Centro, Rinaldi, Kobe, Jiji and Erzinkan) defined in the benchmark problem. To evaluate the performance indices, all the excitations are used at the full intensity. The performance indices larger than one show that the response of the controlled structure is bigger than that of the uncontrolled structure. The performance indices larger than one are highlighted in bold in Tables 3 and 4.

4.1 Study of performance indices

Using system 4 shown in Tables 3 and 4, most of the response quantities are decreased significantly in comparison to the uncontrolled case. The base shears are reduced between 10% and 70% in a majority of earthquakes (i.e., except Jiji in Table 3). The reduction in base displacements is between 26% and 77% in all earthquakes. For the inter-storey drifts, reductions between 10% and 68% are achieved in a majority of earthquakes (i.e., except Jiji in Table 3) in comparison to the uncontrolled case. The floor accelerations are also reduced between 6% and 57% in a majority of earthquakes (i.e., except Jiji in Table 3). The benefit of using system 4 is not only the substantial reduction of base displacements as performance criteria ($J3$) and shears as performance criteria ($J1$), but also the reduction of inter-storey drift ($J4$) and accelerations ($J5$). One of the most important criteria to be considered during strong earthquakes is the reduction of the base displacement ($J3$) of the base-isolated building.

Overall, a controller system that decreases the peak superstructure drift ($J4$) and accelerations ($J5$) while significantly reducing the base displacement ($J3$) and base shear ($J1$) is desirable for a control strategy, and hence the proposed system 4 results in above-mentioned benefits and performs as the best.

4.2 Time-history plots

Figs. 10-12 show the time-history plots of various response quantities for control systems 1 and 2 and 9 and proposed system 4, in FP-X and the FN-Y components of Sylmar earthquake. The reason to select control systems 1 and 2 and 9 is to examine the performance of control system 4 with control systems without NSDs. Fig. 10 presents the plots for the displacement of the center of the base mass in the X direction. The base absolute acceleration in the X direction for control systems 1 and 2 and 9 and proposed system 4 are shown in Fig. 11. Finally, the base

shear in the X direction is presented in Fig. 12. These figures show clearly that the proposed system 4 effectively reduced response quantities in comparison to the control systems 1 and 2 and 9. As shown in Fig. 13, the generated force in system 4 for MR damper used in the location 3 of Fig. 5 is much more less than generated force in two systems 1 and 9 in which NSDs are not used. Fig. 13 also shows that system 4 reduces the generated forces for the same MR damper in comparison to system 2 originally implemented by Narasimhan *et al.* (2006). Fig. 14 expresses the energy level consumed to command MR damper in the location 3 of Fig. 5.

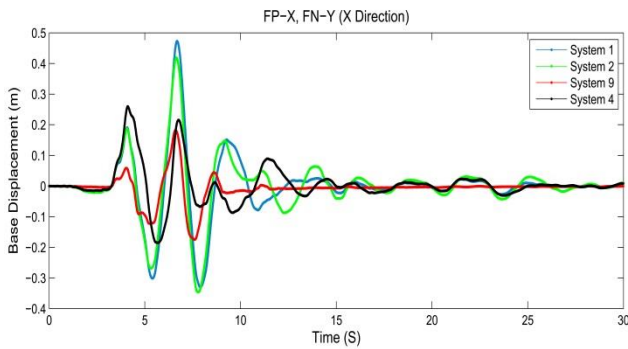


Fig. 10 Base displacement for Sylmar earthquake in direction FP-X FN-Y

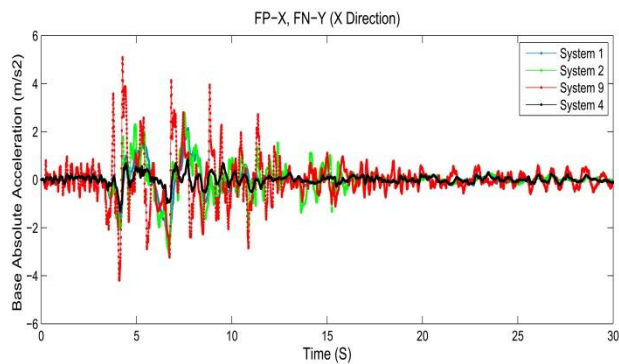


Fig. 11 Base absolute acceleration for Sylmar earthquake in direction FP-X FN-Y

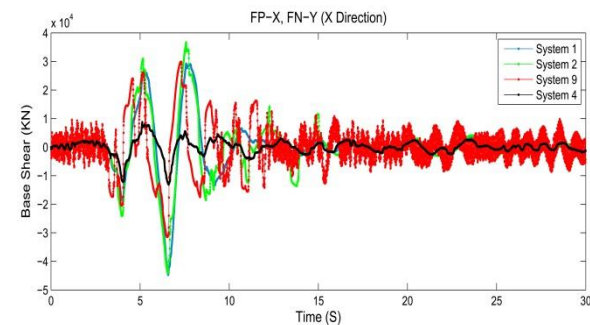


Fig. 12 Base shear for Sylmar earthquake in direction FP-X FN-Y

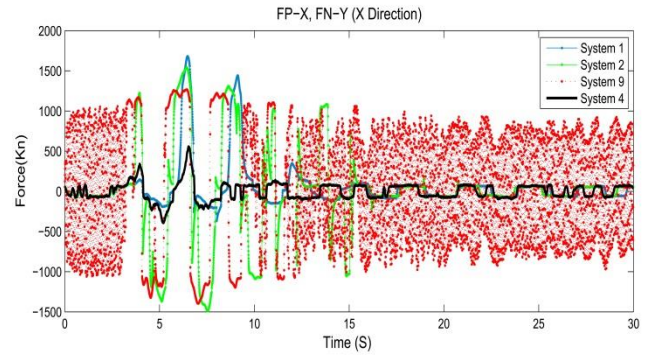


Fig. 13 Generated force in MR damper located in point 3 (X direction) of Fig. 5

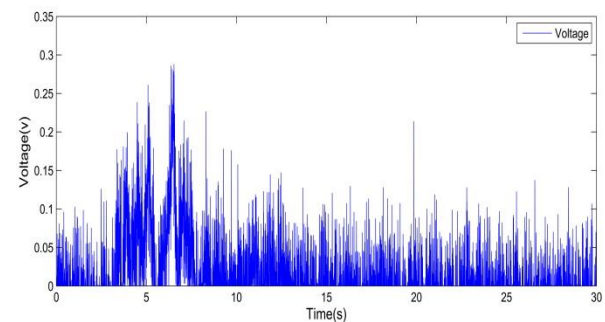


Fig. 14 Voltage consumed to command MR damper in the location 3 (X direction) of Fig. 5

4.3 Comparison between different control systems

Tables 3 and 4 also illustrate that by comparing control systems 1 to 6 in all excitation, control system 4 provides significant performance improvements in reducing all responses. The semi-active velocity controller in the passive-on case combined with MNSD (system 6) and without MNSD (system 9) performs better than the proposed system 4 with respect to the peak base displacement (J_3), and shows performance degradation with respect to the other performance criteria. Also the semiactive velocity controller in passive-off case and combined with MNSD (system 5) almost has better performance than proposed system 4 with respect to the peak absolute floor acceleration (J_5) but shows worse performance with respect to the other performance criteria. The results shown in Figs. 10-12 demonstrate that the proposed system 4 produces improved performance in reducing base displacements and base accelerations and base shears, simultaneously.

5. Conclusions

The base isolators reduce the absolute accelerations and displacements of the superstructure that consequently decrease destructive effects of earthquakes, but can result in large base displacements. The semi-active control devices

which decrease base displacements in the base-isolation systems simultaneously increase the absolute accelerations and drifts of the superstructure. To overcome these issues, we proposed a weakening and regulated damping (WeRD) method. The negative stiffness devices provide desirable negative forces that leads to reduction of the base shear and responses of the superstructure, but if it use lonely, will increase the base displacement. The velocity control algorithm generates initial force for inverse model which creates the required voltage for MR dampers to further regulate damping to reduce base displacement of the structure in a reasonable manner.

The combination of MR damper and NSD as WeRD strategy has been applied to a smart base-isolated benchmark building. The numerical analysis of performance criteria shows that the use of WeRD strategy as control system 4 significantly reduces the displacement, shear, and acceleration responses of the superstructure and the base, using a low energy level.

References

- Attary, N., Symans, M. and Nagarajaiah, S. (2015b), "Development of a rotation-based negative stiffness device for seismic protection of structures", *J. Vib. Control*, **23**(5), 853-867.
- Attary, N., Symans, M., Nagarajaiah, S., Reinhorn, A.M., Constantinou, M.C., Taylor, D., Sarlis, A.A., Pasala, D.T.R. (2013), "Performance assessment of a highway bridge structure employing adaptive negative stiffness for seismic protection", *Structures Congress 2013: Bridging Your Passion with Your Profession*, 1736-1746.
- Attary, N., Symans, M., Nagarajaiah, S., Reinhorn, A.M., Constantinou, M.C., Sarlis, A.A., Pasala, D.T.R. and Taylor, D. (2015), "Performance evaluation of negative stiffness devices for seismic response control of bridge structures via experimental shake table tests", *J. Earthq. Eng.*, **19**(2), 249-276.
- Attary, N., Symans, M., Nagarajaiah, S., Reinhorn, A.M., Constantinou, M.C., Sarlis, A.A., Pasala, D.T.R. and Taylor, D. (2015a), "Numerical simulations of a highway bridge structure employing passive negative stiffness device for seismic protection", *Earthq. Eng. Struct. D.*, **44**(6), 973-995.
- Attary, N., Symans, M.D., Nagarajaiah, S., Reinhorn, A.M., Constantinou, M.C., Taylor, D., Pasala, D.T.R. and Sarlis, A.A. (2012), "Performance evaluation of seismically isolated bridge structure with adaptive passive negative stiffness", *Proceedings of the 15th World Conference on Earthquake Engineering (15WCEE)*.
- Bahar, A., Pozo, F., Acho, L., Rodellar, J. and Barbat, A. (2010), "Parameter identification of large-scale magnetorheological dampers in a benchmark building", *Comput. Struct.*, **88**(3), 198-206.
- Bahar, A., Pozo, F., Acho, L., Rodellar, J. and Barbat, A. (2010), "Hierarchical semi-active control of baseisolated structures using a new inverse model of magnetorheological dampers", *Comput. Struct.*, **88**(7), 483-496.
- Bossis, G., Khuzir, P., Lacin, S. and Volkova, O. (2003), "Yield behavior of magnetorheological suspensions", *J. Magn. Magn. Mater.*, **258**, 456-458.
- Charleson, A.W., Wright, P.D. and Skinner, R.I. (1987), "Wellington central police station, base isolation of an essential facility", *In Pacific Conference on Earthquake Engineering*, 2, 377-388.
- Christopoulos, C., Filiatrault, A. and Bertero, V.V. (2006), "Principles of passive supplemental damping and seismic isolation", *Iuss Press*.
- Dyke, S.J., Spencer, B.F., Sain, M.K. and Carlson, J.D. (1996), "Modeling and control of magnetorheological dampers for seismic response reduction", *Smart Mater. Struct.*, **5**(5), 565.
- Dyke, S.J., Spencer, B.F., Sain, M.K. and Carlson, J.D. (1998), "An experimental study of MR dampers for seismic protection", *Smart Mater. Struct.*, **7**(5), 693.
- Hall, J.F., Heaton, T.H. and Halling, M.W. (1995), "Near-source ground motion and its effects on flexible buildings", *Earthq. Spectra*, **11**(4), 569-605.
- Iemura, H. and Pradono, M.H. (2009), "Advances in the development of pseudo-negative-stiffness dampers for seismic response control", *Struct. Control Health Monit.*, **16**(7-8), 784-799.
- Jangid, R.S. and Kelly, J.M. (2001), "Base isolation for near-fault motions", *Earthq. Eng. Struct. D.*, **30**(5), 691-707.
- Jung, H.J., Choi, K.M., Spencer, B.F. and Lee, I.W. (2006), "Application of some semi-active control algorithms to a smart base-isolated building employing MR dampers", *Struct. Control Health Monit.*, **13**(2-3), 693-704.
- Kelly, J.M. (1999), "The role of damping in seismic isolation", *Earthq. Eng. Struct. D.*, **28**(1), 3-20.
- Makris (1997), "Rigidity-plasticity-viscosity: can electrorheological dampers protect base-isolated structures from near-source ground motions?", *Earthq. Eng. Struct. D.*, **25**(6), 571-592.
- Naeim, F. and Kelly, J.M. (1999), "Design of seismic isolated structures: from theory to practice", *John Wiley & Sons*.
- Nagarajaiah, S. and Narasimhan, S., "Smart base-isolated benchmark building. Part II: phase I sample controllers for linear isolation systems", *Struct. Control Health Monit.*, **16**(2-3), 589-604.
- Nagarajaiah, S., Reinhorn, A., Constantinou, M., Taylor, D., Pasala, D.T. and Sirilis, A.A. (2010), "Adaptive negative stiffness: a new structural modification approach for seismic protection", *Proceedings of the 5th World Conference on Structural Control and Monitoring*, Tokyo, Japan.
- Narasimhan, S., Nagarajaiah, S., Johnson, E.A. and Gavin, H.P. (2006), "Smart base-isolated benchmark building. Part I: problem definition", *Struct. Control Health Monit.*, **13**(2-3), 573-588.
- Pasala, D.T., Sarlis, A.A., Nagarajaiah, S., Reinhorn, A.M., Nagarajaiah, S., Constantinou, M.C. and Taylor, D. (2012), "Adaptive negative stiffness: New structural modification approach for seismic protection", *J. Struct. Eng.*, **139**(7), 1112-23.
- Reinhorn, A.M., Viti, S. and Cimellaro, G. (2005), "Retrofit of structures: Strength reduction with damping enhancement", *Proceedings of the 37th UJNR panel meeting on wind and seismic effects*.
- Sarlis, A.A., Pasala, D.T., Constantinou, M.C., Reinhorn, A.M., Nagarajaiah, S. and Taylor, D. (2011), "Negative stiffness device for seismic protection of structures—an analytical and experimental study", *In COMPDYN 2011, Proceedings of the 3rd ECCOMAS Thematic Conference on Computational Methods in Structural Dynamics and Earthquake Engineering*, Corfu, Greece.
- Sarlis, A.A., Pasala, D.T., Constantinou, M.C., Reinhorn, A.M., Nagarajaiah, S. and Taylor, D. (2012), "Negative stiffness device for seismic protection of structures", *J. Struct. Eng.*, **139**(7), 1124-1133.
- Skinner, R.I., Robinson, W.H. and McVerry, G.H. (1993), "An introduction to seismic isolation", *John Wiley & Sons*.
- Soong, T.T. (1990), "Active structural control: theory and application", *New York: Long-an Scientific and Technical Publishing*.

- Sorace, S. and Terenzi, G. (2008), "Analysis and demonstrative application of a base isolation/supplemental damping technology", *Earthq. Spectra*, **24**(3), 775-793.
- Spencer, B.F., Dyke, S.J. and Sain, M.K. (1996), "Magnetorheological dampers: a new approach to seismic protection of structures", *In Decision and Control, 1996., Proceedings of the 35th IEEE Conference on (Vol. 1, pp. 676-681). IEEE.*
- Viti, S., Cimellaro, G. and Reinhorn, A.M. (2006), "Retrofit of a hospital through strength reduction and enhanced damping", *Smart Struct. Syst.*, **2**(4), 339-355.
- Yang, G. (2001), "Large-scale magnetorheological fluid damper for vibration mitigation: modeling, testing and control".

CC

A. Evaluation criteria

1. Peak base shear (isolation-level) in the controlled structure normalized by the corresponding shear in the uncontrolled structure

$$J_1(q) = \max_t \|V_0(t, q)\| / \max_t \|V_0^{\wedge}(t, q)\|$$

2. Peak base displacement or isolator deformation in the controlled structure normalized by the corresponding displacement in the uncontrolled structure

$$J_3(q) = \max_{t,i} \|d_i(t, q)\| / \max_{t,i} \|d_i^{\wedge}(t, q)\|$$

3. Peak inter-story drift in the controlled structure normalized by the corresponding inter-story drift in the uncontrolled structure

$$J_4(q) = \max_{t,f} \|d_f(t, q)\| / \max_{t,f} \|d_f^{\wedge}(t, q)\|$$

4. Peak absolute floor acceleration in the controlled structure normalized by the corresponding acceleration in the uncontrolled structure

$$J_5(q) = \max_{t,f} \|a_f(t, q)\| / \max_{t,f} \|a_f^{\wedge}(t, q)\|$$

5. RMS absolute floor acceleration in the controlled structure normalized by the corresponding RMS acceleration in the uncontrolled structure

$$J_8(q) = \max_f \|\sigma_a(t, q)\| / \max_f \|\sigma_a^{\wedge}(t, q)\|$$

Table 3 Performance indexes in direction FP-X FN-Y for nine systems

Performance Index	Earthquake							
	System	Newhall	Sylmar	El Centro	Rinaldi	Kobe	jiji	Erzinkan
J1	1	0.9150	0.8454	0.9185	1.0962	0.8206	0.8018	0.8390
	2	0.9719	0.9014	1.2489	1.0461	1.0435	0.8350	0.9284
	3	1.1669	0.4282	0.7075	0.6843	0.2371	1.4585	0.5539
	4	0.5885	0.4619	0.3485	0.6460	0.3409	1.0113	0.3416
	5	0.9391	0.5216	0.2724	0.6465	0.3091	1.2806	0.4411
	6	0.7454	0.5936	0.9785	0.7919	0.6827	0.8407	0.7368
	7	0.8496	0.9343	0.948	0.9707	0.8613	0.8634	1.0122
	8	0.8906	0.3718	0.3094	0.5014	0.1768	1.1534	0.4646
	9	0.9265	0.8775	1.0297	0.9912	0.8623	0.7219	0.9552
J3	1	0.6005	0.8459	0.4323	0.7369	0.4603	0.7030	0.5517
	2	0.5597	0.7309	0.5431	0.5962	0.5182	0.6507	0.4655
	3	1.0870	0.5844	0.6227	0.6019	0.4116	1.3659	0.5047
	4	0.6124	0.5651	0.3871	0.4575	0.4138	0.7462	0.3343
	5	0.8537	0.6494	0.3942	0.5597	0.4349	0.9359	0.4072
	6	0.4683	0.4712	0.1478	0.4617	0.2457	0.5467	0.3838
	7	0.6945	0.9034	0.7295	0.9141	0.6772	0.7506	0.6840
	8	0.8588	0.4944	0.4508	0.4835	0.4011	1.1222	0.3906
	9	0.3881	0.5386	0.1193	0.4194	0.2453	0.4953	0.3745
J4	1	0.9261	0.8477	0.7842	1.0967	0.8587	0.8217	0.8097
	2	1.0283	0.8662	1.2550	0.9623	0.9966	0.8561	0.8634
	3	1.2047	0.3648	0.5420	0.6097	0.2878	1.5890	0.6144
	4	0.6230	0.5321	0.3189	0.6765	0.5804	1.0119	0.3854
	5	0.9787	0.4915	0.2558	0.6075	0.4833	1.3357	0.4891
	6	1.7746	1.0818	1.8631	1.1119	1.6459	0.9138	0.9515
	7	0.8396	0.9191	0.7873	0.9238	0.7641	0.8547	0.8705
	8	0.8952	0.4143	0.3062	0.4765	0.2283	1.1278	0.4272
	9	1.6148	1.0296	1.7832	1.0436	1.6928	0.8874	0.9919
J5	1	1.0563	1.0201	0.8646	1.1811	1.1512	0.8478	0.8751
	2	1.4753	1.1588	1.6089	1.0102	1.6313	0.8728	1.2325
	3	1.1828	0.4882	0.6598	0.5944	0.6961	1.7161	0.5884
	4	0.8078	0.7051	0.5919	0.7261	0.8553	1.0356	0.4360
	5	1.3798	0.6241	0.4649	0.6552	0.5695	1.4390	0.5658
	6	2.8403	2.2241	4.4673	1.9994	3.7300	1.2599	1.9937
	7	0.8678	0.9731	0.8671	0.9904	0.9686	0.8606	1.0123
	8	0.9046	0.6368	0.5522	0.5686	0.4595	1.1968	0.5624
	9	2.8483	2.1872	4.3483	1.9083	3.4431	1.3628	2.0745
J8	1	0.7221	0.6854	0.5323	0.6270	0.5814	0.6483	0.5802
	2	0.8944	0.7367	0.7656	0.7147	0.7294	0.7184	0.6261
	3	1.0393	0.3579	0.4866	0.4786	0.2132	1.4225	0.3932
	4	0.5161	0.3832	0.3390	0.3683	0.3778	0.6980	0.2307
	5	0.6630	0.3943	0.2920	0.4060	0.2756	1.0927	0.2734
	6	1.5964	1.2223	2.0631	1.3065	1.5481	1.1344	0.9242
	7	0.7091	0.8027	0.6079	0.6781	0.5632	0.8179	0.7140
	8	0.5980	0.2797	0.2910	0.3219	0.2069	0.9034	0.2762
	9	1.6033	1.2501	2.1191	1.3284	1.5465	1.1401	0.8555

Table 4 Performance indexes in direction FP-Y FN-X for nine systems

Performance Index	Earthquake							
	System	Newhall	Sylmar	El Centro	Rinaldi	Kobe	jiji	Erzinkan
J1	1	0.8315	0.7622	0.9204	1.0109	0.9705	0.7156	0.7505
	2	0.8825	0.8049	1.2659	0.9773	1.1512	0.7359	0.8393
	3	1.0906	0.3880	0.7161	0.6608	0.2628	1.5365	0.4731
	4	0.5173	0.3817	0.3584	0.5945	0.4304	0.9042	0.3007
	5	0.8374	0.4980	0.2906	0.6144	0.3808	1.3039	0.3811
	6	0.6406	0.4960	1.0186	0.7411	0.8231	0.7366	0.6616
	7	0.7755	0.9432	0.9811	0.8823	0.9822	0.7722	0.9187
	8	0.7382	0.3167	0.3481	0.3982	0.4490	1.0230	0.4259
	9	0.8568	0.7859	1.0195	0.9226	1.0624	0.6368	0.8287
J3	1	0.6186	0.7744	0.6037	0.6335	0.5062	0.6686	0.5187
	2	0.5498	0.7392	0.6266	0.6177	0.5265	0.6331	0.5023
	3	1.0952	0.5430	0.9520	0.6310	0.4284	1.1255	0.4780
	4	0.5724	0.5328	0.5744	0.4896	0.4270	0.6598	0.3628
	5	0.8044	0.6287	0.5793	0.6072	0.4480	0.8744	0.4097
	6	0.4990	0.4557	0.1590	0.4986	0.2490	0.5008	0.4245
	7	0.6082	0.8505	0.8218	0.6910	0.7232	0.7217	0.6353
	8	0.7889	0.4742	0.7025	0.4814	0.4201	0.7386	0.4184
	9	0.4049	0.5775	0.1415	0.4360	0.2670	0.4670	0.4379
J4	1	1.0541	0.7342	0.9612	1.1204	0.9665	0.6980	0.7826
	2	1.2390	0.7883	1.5910	0.9885	1.3333	0.7262	0.8937
	3	1.1969	0.4278	0.6978	0.6122	0.2982	1.7198	0.5239
	4	0.5553	0.4838	0.4770	0.6587	0.5412	0.9056	0.3691
	5	0.9017	0.5615	0.3859	0.5709	0.3525	1.4424	0.4383
	6	1.4967	0.8155	3.3672	0.9375	1.9171	0.8266	0.8366
	7	0.7419	0.8689	0.9579	0.9147	0.9436	0.7570	0.9452
	8	0.7353	0.3976	0.3702	0.3962	0.2261	1.0999	0.4643
	9	1.7182	0.8530	3.3671	0.9872	1.8745	0.6731	0.9597
J5	1	1.1349	0.8793	1.0056	1.1768	0.9650	0.7101	0.7997
	2	1.3972	0.9263	2.0893	1.0199	1.4686	0.8027	1.1372
	3	1.0889	0.4814	0.6778	0.5849	0.3300	1.9811	0.5523
	4	0.6863	0.5694	0.8039	0.6908	0.6903	0.9442	0.5626
	5	0.8124	0.6359	0.7447	0.5971	0.8417	1.5895	0.5247
	6	2.1866	2.1281	4.4110	1.8038	3.3491	0.9199	1.9514
	7	0.7546	0.8866	1.0586	0.9545	0.9117	0.7642	0.9513
	8	0.6983	0.4635	0.4994	0.4010	2.1401	1.2044	0.5062
	9	2.3883	2.2292	4.4114	1.7067	3.3235	0.9197	1.9499
J8	1	0.7363	0.5481	0.6855	0.4756	0.7160	0.5686	0.4986
	2	0.8388	0.6121	0.9872	0.4752	0.9762	0.6089	0.5141
	3	1.1435	0.2819	0.6317	0.3536	0.2565	1.5523	0.2983
	4	0.5090	0.2769	0.4218	0.2632	0.4861	0.6124	0.1764
	5	0.6685	0.3201	0.3974	0.2986	0.3832	1.1571	0.2060
	6	1.5641	0.8511	2.8110	0.8746	2.0131	0.8813	0.6308
	7	0.6298	0.6937	0.6961	0.5003	0.6980	0.6808	0.6111
	8	0.5386	0.2180	0.4251	0.2100	0.2480	0.7978	0.2084
	9	1.5920	0.8904	2.8136	0.8618	1.9989	0.8845	0.6520